ACS Partner Journal

CHEM & BIO ENGINEERING

pubs.acs.org/ChemBioEng

Article

Hydrostable Fluorinated Metal–Organic Frameworks for CO_2 Capture from a Wet Flue Gas: Multiscale Computational Screening

Published as part of Chem & Bio Engineering special issue "Framework Materials".

Athulya S. Palakkal, Saad Aldin Mohamed, and Jianwen Jiang*

Cite This: *Chem Bio Eng.* 2024, 1, 970–978

Read Online

ACCESS | Metrics & More | Article Recommendations | Supporting Information

ABSTRACT: Metal–organic frameworks (MOFs) are promising adsorbents for CO_2 capture due to readily tunable porosity and diverse functionality; however, their performance is deteriorated by the presence of H_2O in a flue gas. Fluorinated MOFs (FMOFs) may impede H_2O interaction with frameworks and enhance CO_2 adsorption under humid conditions. In this study, a multiscale computational screening study is reported to identify the top FMOFs for CO_2 capture from a wet flue gas. Initially, geometric properties as well as heats of H_2O adsorption are used to shortlist FMOFs with a suitable pore size and weak H_2O affinity. Then, grand-canonical Monte Carlo simulations are conducted for adsorption of a $CO_2/N_2/H_2O$ mixture with 60% relative humidity in 5061 FMOFs. Based on the adsorption performance, 19 FMOFs are identified as top candidates. It is revealed that the position of F atom, rather than the amount, affects CO_2 adsorption; moreover, N-decorated FMOFs are preferential for selective CO_2 adsorption. Finally, the hydrostability of the top FMOFs is confirmed by first-principles molecular dynamics simulations. From a microscopic level, this study provides quantitative structure–performance relationships, discovers hydrostable FMOFs with high CO_2 capture performance from a wet flue gas, and would facilitate the development of new MOFs toward efficient CO_2 capture under humid conditions.

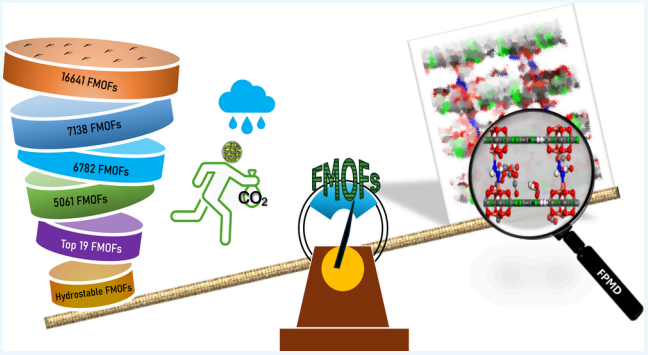

KEYWORDS: *metal–organic frameworks, CO_2 capture, adsorption, Monte Carlo simulation, molecular dynamics simulation, hydrostability*

1. INTRODUCTION

Rapid increase of CO_2 emissions is considered the primary reason for global warming and climate change.[1,2] Several technologies have been proposed for CO_2 capture including amine sorption, cryogenic distillation, membrane separation, and solid adsorption.[3,4] As a special class of nanoporous materials, metal–organic frameworks (MOFs) have emerged as promising adsorbents for the capture of CO_2 from flue gas.[5−8] Consisting of metal nodes and organic linkers, MOFs are extended networks with a wide range of surface areas, pore volumes, and functional groups. Although MOFs have been extensively examined for CO_2 capture, their performance is severely reduced by H_2O in a wet flue gas.[9,10] Therefore, there has been considerable interest in developing MOFs that can maintain CO_2 capture performance under humid conditions.

To date, a great number of MOFs have been synthesized experimentally and generated computationally.[11,12] High-throughput computational screening is an effective way to identify promising MOFs for gas adsorption and separation, particularly for CO_2 capture. For instance, adsorption of CO_2, N_2, and CH_4 in 137 953 hypothetical MOFs (hMOFs) was simulated, and the relationships between structural characteristics and performance criteria were established toward CO_2/N_2 and CO_2/CH_4 separation.[13] Based on the adsorption, diffusion, and permeation of CO_2, N_2, and CH_4, 137 953 hMOFs were screened for single-step membrane separation of a $CO_2/N_2/CH_4$ mixture.[14] Hydrophobic computation-ready experimental (CoRE) MOFs were shortlisted for separation of CO_2 and H_2S from a $CH_4/C_2H_6/C_3H_8/H_2S/CO_2/H_2O$ mixture.[15] The Cambridge Structural Database (CSD) MOFs were screened for CO_2 capture, and a handful of MOFs were identified to possess selective adsorption and molecular sieving capabilities.[16] About ∼20 000 hMOFs with diverse metal nodes, organic linkers, functional groups, and pore geometries were designed and assessed for post-combustion CO_2

Received: May 31, 2024
Revised: October 16, 2024
Accepted: October 20, 2024
Published: October 29, 2024

https://doi.org/10.1021/cbe.4c00111
Chem Bio Eng. 2024, 1, 970–978

capture.[17] From a library of over 300 000 hMOFs, different CO_2 binding sites were classified, and water-stable MOFs were identified and further synthesized.[18]

Most of the aforementioned screening studies for CO_2 capture were focused on dry flue gas without considering the effect of humidity. Practically, H_2O is ubiquitously present in a flue gas, and its effect must be taken into account. Among different subclasses of MOFs, fluorinated MOFs (FMOFs) possess unique properties such as high electronegativity, low electric polarizability, hydrophobicity, and selective adsorption. The hydrophobic nature of FMOFs was demonstrated by confining water clusters in a FMOF, namely $[Ag_6(tz)_6]$ (tz = 3,5-bis(trifluoromethyl)-1,2,4-triazolate).[19] With these salient features, FMOFs have been highly regarded as intriguing materials for CO_2 capture under humid conditions.[20] Notably, Eddaoudi and co-workers designed a series of FMOFs, based on inorganic fluorinated anions (e.g., MF_6^{2-} and MOF_5^{2-}), with exceptional CO_2 capture capability in the presence of H_2O.[21−23] NU-1000 functionalized with perfluoroalkanes of various chain lengths (C_1−C_9) was shown to selectively adsorb CO_2 with moderate to high heat of adsorption.[24] Decorated with $-CF_3$ groups in channels and pockets, superhydrophobic FMOF-1 was found to exhibit high CO_2 adsorption even in the presence of 80% relative humidity.[25] Increased CO_2 uptake and CO_2/N_2 selectivity were observed with increasing number of F atoms by stepwise fluorination in ultramicroporous MOFs.[26]

Considering the large number of FMOFs available in the literature, the full potential of FMOFs for CO_2 capture under humid conditions has not been thoroughly investigated. The objective of this study is to computationally screen potential candidates from a diverse collection of FMOFs for CO_2 capture from wet flue gas. Altogether, 16 641 FMOFs were collected from three different databases: 936 from an anion-pillared MOF database,[27] 213 from the CoRE-MOF database,[28] and 15 492 from the hMOF database.[12] Figure 1 illustrates the most common metal nodes in these FMOFs. In addition to high CO_2 capture performance, the potential candidates should also be hydrostable and abstain from degradation in a humid environment. To quantify hydrostability, we examined the structural integrity of top candidates by using first-principles molecular dynamics (FPMD) simulation. In this context, this study adopts a multiscale approach synergizing molecular scale and electronic-structure scale.

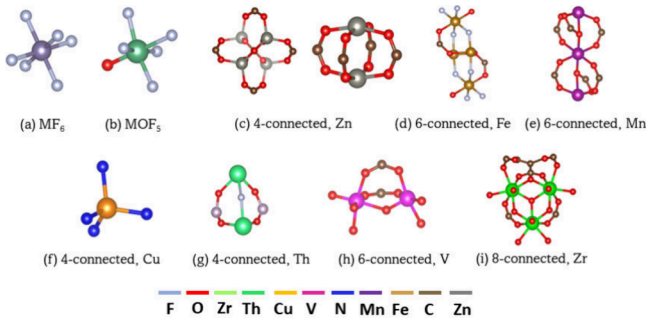

Figure 1. Most common metal nodes in FMOFs: (a−b) from an anion-pillared MOF database,[27] (c−e) from the CoRE-MOF database,[28] and (f−i) from the hMOF database.[12]

2. COMPUTATIONAL METHODOLOGY

2.1. Workflow. Figure 2 illustrates the workflow to identify top FMOFs for CO_2 capture from a wet flue gas, consisting of five steps. (i) All the 16 641 FMOFs were geometrically characterized by pore limiting diameter (PLD), largest cavity diameter (LCD), and porosity (ϕ) as estimated via Zeo++.[29] Considering the kinetic diameters of CO_2 (3.30 Å), N_2 (3.64 Å), and H_2O (2.65 Å), 7138 structures with PLD ranging from 2.7 to 6.0 Å were selected. (ii) FMOFs with coordinatively open metal sites tend to strongly interact with H_2O and thus are not ideal for CO_2 adsorption in a humid condition; consequently, these FMOFs were detected via OMS detector[28] and excluded. (iii) 6782 FMOFs from step (ii) were evaluated for H_2O affinity. Specifically, canonical Monte Carlo simulation was conducted for a single H_2O molecule in each MOF, and the heat of H_2O adsorption Q_{st}^{o} at 298 K was calculated. Those with Q_{st}^{o} > 42 kJ/mol (i.e., the enthalpy of water vaporization) were considered relatively hydrophilic and discarded, resulting in 5061 FMOFs. (iv) Adsorption of a ternary gas mixture $CO_2/N_2/H_2O$ in the 5061 FMOFs was calculated at 298 K via grand-canonical Monte Carlo (GCMC) simulation method. Based on the adsorption performance, top 19 FMOFs were identified. (v) Finally, the hydrostability of the top 19 FMOFs was evaluated through FPMD simulation.

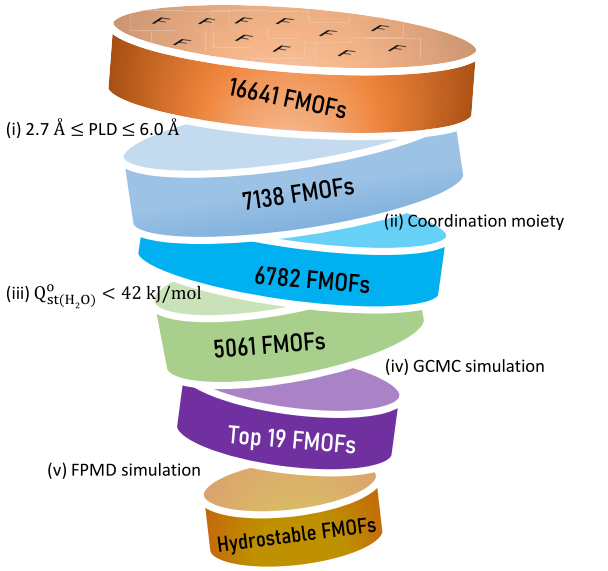

Figure 2. Workflow to identify top FMOFs for CO_2 capture from a wet flue gas.

2.2. Simulation Models and Methods. CO_2 capture from a wet flue gas (mimicked by a ternary gas mixture of $CO_2/N_2/H_2O$) in the 5061 FMOFs was simulated via GCMC method. The framework atoms were described by a combination of Lennard-Jones (LJ) and electrostatic potential

$$4\varepsilon_{ij}\left[\left(\frac{\sigma_{ij}}{r_{ij}}\right)^{12}-\left(\frac{\sigma_{ij}}{r_{ij}}\right)^{6}\right]+\frac{q_i q_j}{4\pi\varepsilon_0 r_{ij}} \quad (1)$$

where σ_{ij} and ε_{ij} are the LJ potential collision diameter and well depth, r_{ij} is the distance between atoms i and j, q_i is the atomic charge, and $\varepsilon_0 = 8.8542 \times 10^{-12}$ C^2 N^{-1} m^{-2} is the permittivity of vacuum. The LJ potential parameters were adopted from the universal force field (UFF)[30] and Dreiding force field.[31] For

https://doi.org/10.1021/cbe.4c00111
Chem Bio Eng. 2024, 1, 970−978

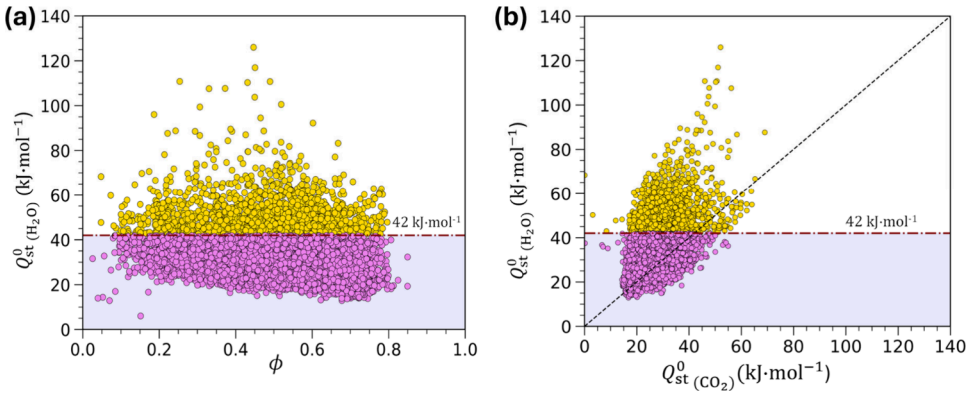

Figure 3. (a) $Q^o_{st(H_2O)}$ versus void fraction ϕ and (b) $Q^o_{st(H_2O)}$ versus $Q^o_{st(CO_2)}$ in 6782 FMOFs at 298 K.

cross LJ interactions, the potential parameters were estimated by the Lorentz–Berthelot mixing rules. The atomic charges were evaluated from the PACMOF method.[32] CO_2 and N_2 were described by the transferable potentials for phase equilibria (TraPPE) force field.[33] H_2O was mimicked by the four-site TIP4P model,[34] as it fairly well predicts the saturation pressure of water at 298 K (4.37 kPa) among different models.[35]

In each of the 5061 FMOFs, GCMC simulation was run at 298 K for 2×10^4 cycles (10^4 for equilibration and 10^4 for production). The total pressure of the $CO_2/N_2/H_2O$ mixture was 1 bar with a composition of 0.124/0.850/0.026. The partial pressure of H_2O was 2.6 kPa, corresponding to a relative humidity of 60% for the TIP4P water model. Adsorbate molecules were subjected to four types of trial moves including translation, rotation, creation/deletion, and identity exchange. Each cycle consisted of N trial moves (N: the number of adsorbate molecules; N = 20 if the number <20). The framework was considered rigid with atoms frozen during simulation. The LJ interactions were calculated with a cutoff of 12.8 Å, while the electrostatic interactions were estimated using Ewald summation. All the GCMC simulations were performed using the RASPA package.[36] Based on adsorption performance, top 19 FMOFs were identified. In each top FMOF, a longer GCMC simulation with 10^5 cycles (5×10^4 for equilibration and 5×10^4 for production) was further conducted for the adsorption of the $CO_2/N_2/H_2O$ mixture.

The hydrostability of the top 19 FMOFs in the presence of coadsorbed CO_2, N_2, and H_2O was examined by FPMD simulation using the CP2K package.[37] In each of the top FMOF, the numbers and initial configurations of CO_2, N_2, and H_2O were generated from GCMC simulation. The Perdew–Burke–Ernzerhof (PBE) functional[38,39] was adopted with dispersion interactions treated at the DFT-D3 level.[40] For elements such as carbon, oxygen, hydrogen, and nitrogen, the triple ζ (TZVP-MOLOPT-GTH) basis set was utilized, while the double ζ (DZVP-MOLOPT-SR-GTH) was utilized for metal atoms (copper, zinc, iron, and vanadium). For each FMOF, FPMD simulation was performed in an isothermal and isobaric ensemble at 298 K and 1 bar. The temperature and pressure were controlled by velocity rescaling scheme with a time constant of 0.1 ps and by a barostat with a time constant of 1 ps, respectively. A time step of 1 fs was applied to integrate the equations of motion, and the simulation duration was 5 ps. During FPMD simulation, the PLD was estimated as a function of time.

3. RESULTS AND DISCUSSION

First, we present H_2O affinity in 6782 FMOFs and the adsorption performance of the $CO_2/N_2/H_2O$ mixture in 5061 FMOFs. Based on a trade-off between adsorption capacity and selectivity, 19 FMOFs are shortlisted as top candidates for CO_2 capture. Then, we characterize the structures and chemical constituents (including F, N, and metal atoms) in the top FMOFs. Finally, the hydrostability and CO_2–framework interaction in these top FMOFs are analyzed.

3.1. H_2O Affinity and Adsorption Performance. Figure 3a shows the heat of H_2O adsorption at infinite dilution $Q^o_{st(H_2O)}$ versus porosity ϕ in 6782 MOFs. Several MOFs exhibit very high $Q^o_{st(H_2O)}$ values of over 100 kJ/mol when ϕ is around 0.5, indicating strong H_2O affinity and hence not suitable for CO_2 capture in the presence of humidity. A handful of MOFs have $Q^o_{st(H_2O)}$ below 20 kJ/mol when ϕ is <0.2 or >0.7, suggesting H_2O adsorption is not strong when ϕ is too low in a MOF with insufficient pore volume or when ϕ is too high in a MOF with weak guest–host interaction. If a threshold of 42 kJ/mol (i.e., enthalpy of water vaporization) is set, 5061 MOFs with $Q^o_{st(H_2O)}$ < 42 kJ/mol can be selected as relatively hydrophobic. From Figure 3b for $Q^o_{st(H_2O)}$ versus $Q^o_{st(CO_2)}$, we observe that many selected MOFs (approximately 2000) have higher affinity for CO_2 than H_2O (i.e., $Q^o_{st(CO_2)} > Q^o_{st(H_2O)}$). One may use these MOFs for screening in step (iv). However, we attempted to use all the 5061 MOFs with $Q^o_{st(H2O)}$ < 42 kJ/mol for screening to avoid possibly missing potential candidates.

The separation performance of 5061 MOFs for CO_2 capture from the $CO_2/N_2/H_2O$ mixture at 298 K and 1 bar is quantified by the adsorption capacity of CO_2 (N_{CO_2}), as well as the adsorption selectivity of CO_2 over N_2 (S_{CO_2/N_2}) and over H_2O (S_{CO_2/H_2O}), respectively. The selectivity is defined as

$$S_{x/y} = \frac{N_x/p_x}{N_y/p_y} \tag{2}$$

where N_x and N_y are the adsorption capacities of components x and y, respectively, while p_x and p_y are the partial pressures. If an adsorbent has a high adsorption capacity, then its selectivity is usually low. To counterbalance, a trade-off (TSN) is further used to assess CO_2/N_2 separation performance

$$\mathrm{TSN} = N_{CO_2} \log(S_{CO_2/N_2}) \tag{3}$$

https://doi.org/10.1021/cbe.4c00111
Chem Bio Eng. 2024, 1, 970–978

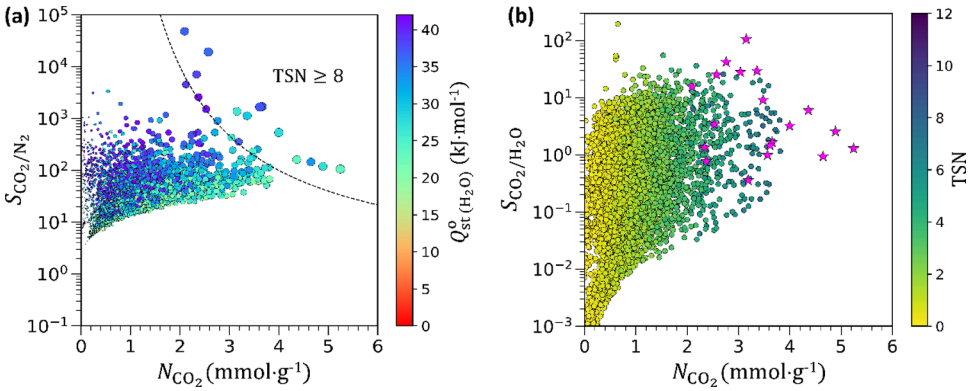

Figure 4. (a) S_{CO_2/N_2} versus N_{CO_2} in 5061 FMOFs. The symbol size corresponds to the magnitude of TSN, the dashed line denotes TSN = 8, and the color scaling denotes different values of $Q^o_{st(H_2O)}$. (b) S_{CO_2/H_2O} versus N_{CO_2} in 5061 FMOFs. The FMOFs with TSN ≥ 8 are denoted by ★. The color scaling denotes different TSN.

Table 1. Structural and Adsorption Properties of Top 19 FMOFs[a]

no.	FMOF	PLD (Å)	LCD (Å)	ϕ	N_{CO_2} (mmol·g^{-1})	N_{H_2O} (mmol·g^{-1})	S_{CO_2/N_2}	S_{CO_2/H_2O}
1	hMOF-5063923	2.75	3.75	0.23	3.44	0.52	1626.58	1.36
2	hMOF-5063926	2.75	3.75	0.23	3.49	0.48	1614.89	1.50
3	hMOF-16702	2.75	3.75	0.19	2.54	0.02	18244.60	23.70
4	hMOF-1002454	3.25	3.75	0.46	3.90	0.11	519.70	7.29
5	hMOF-35835	4.25	5.75	0.70	2.41	10.09	101.66	0.05
6	hMOF-28562	2.75	3.75	0.25	3.28	0.02	1095.20	27.10
7	hMOF-26522	3.75	4.75	0.59	4.13	1.84	117.36	0.46
8	hMOF-27207	3.75	4.25	0.61	2.19	7.54	164.28	0.06
9	hMOF-28016	2.75	3.75	0.26	3.01	0.006	1255.80	99.82
10	hMOF-5033915	2.75	3.25	0.14	2.02	0.02	47708.30	15.16
11	hMOF-36835	3.25	4.75	0.56	4.14	0.14	158.28	5.96
12	hMOF-31797	2.75	3.75	0.18	2.28	0.37	6806.88	1.26
13	hMOF-24459	3.75	4.75	0.54	3.32	1.03	244.60	0.67
14	hMOF-34259	3.25	4.25	0.49	3.38	0.08	229.06	8.77
15	hMOF-5033608	3.25	3.75	0.22	2.71	0.01	886.28	39.59
16	hMOF-34934	3.25	4.25	0.52	3.01	1.88	347.88	0.33
17	hMOF-1002619	2.75	4.25	0.25	2.25	0.61	2519.77	0.76
18	VOFFIVE-3_Fe	3.31	4.63	0.20	2.52	0.13	1827.25	4.07
19	hMOF-36776	3.25	3.75	0.31	2.87	0.02	405.54	27.72

[a]The adsorption properties are based on longer GCMC simulations, different from Figure 4.

Figure 4a shows S_{CO_2/N_2} versus N_{CO_2} in 5061 FMOFs. If plotted in terms of different databases, out of 5061 FMOFs, 4901 are from the hMOF database, 140 are from the anion-pillared MOF database, and 20 are from the CoRE MOF database (Figure S1). At a small N_{CO_2}, a wide range of S_{CO_2/N_2} is observed from 0.1 to 10^5. The high S_{CO_2/N_2} is attributed to the strong surface potential overlap and favorable adsorption of CO_2 in small pores. Generally, N_{CO_2} rises with increasing pore size; meanwhile, S_{CO_2/N_2} drops and tends to approach a constant because CO_2 adsorption becomes weak in large pores. For most of the FMOFs plotted in Figure 4a, Q^o_{st} is between 20 and 42 kJ/mol. FMOFs with high TSN, rather than solely high S_{CO_2/N_2} or N_{CO_2}, are appealing to CO_2 capture. Moving toward the right-top corner, TSN becomes greater. If we set TSN ≥ 8, 19 FMOFs can be shortlisted as top candidates. These FMOFs possess N_{CO_2} from 2.09 to 5.24 mmol·g^{-1} and very high S_{CO_2/N_2} from 106 to 48 043. Shown in Figure 4b is S_{CO_2/H_2O} versus N_{CO_2} in 5061 FMOFs. The general trend is that S_{CO_2/H_2O} rises with N_{CO_2}. FMOFs with great TSN exhibit large N_{CO_2} but either low or high S_{CO_2/H_2O}. Specifically, the top 19 FMOFs shortlisted based on TSN have S_{CO_2/H_2O} in the range from 0.35 to 106.

3.2. Characteristics of Top FMOFs. Table 1 summarizes the structural and adsorption properties in the top 19 FMOFs with their crystal structures listed in Table S1. All of these FMOFs are hypothetical with PLD ranging from 2.75 to 4.25 Å. The porosity ϕ is mostly populated between 0.2 and 0.3, with a few beyond 0.5. This suggests that microporous FMOFs are preferable for CO_2 capture under humid conditions. Among the 19 MOFs, hMOF-5063923 and hMOF-5063926 are two configurational isomers with different arrangements of F atoms across C═C bond. They exhibit similar CO_2 adsorption capacity N_{CO_2} (3.44 and 3.49 mmol·g^{-1}) and selectivity S_{CO_2/N_2} (1626.58 and 1614.89). Generally, N_{CO_2} values in the 19 FMOFs are between 2.02 and 4.14 mmol·g^{-1}. The highest N_{CO_2} (4.14 and 4.13 mmol·g^{-1}) are observed in hMOF-36835 and hMOF-26522, meanwhile, with an

https://doi.org/10.1021/cbe.4c00111
Chem Bio Eng. 2024, 1, 970−978

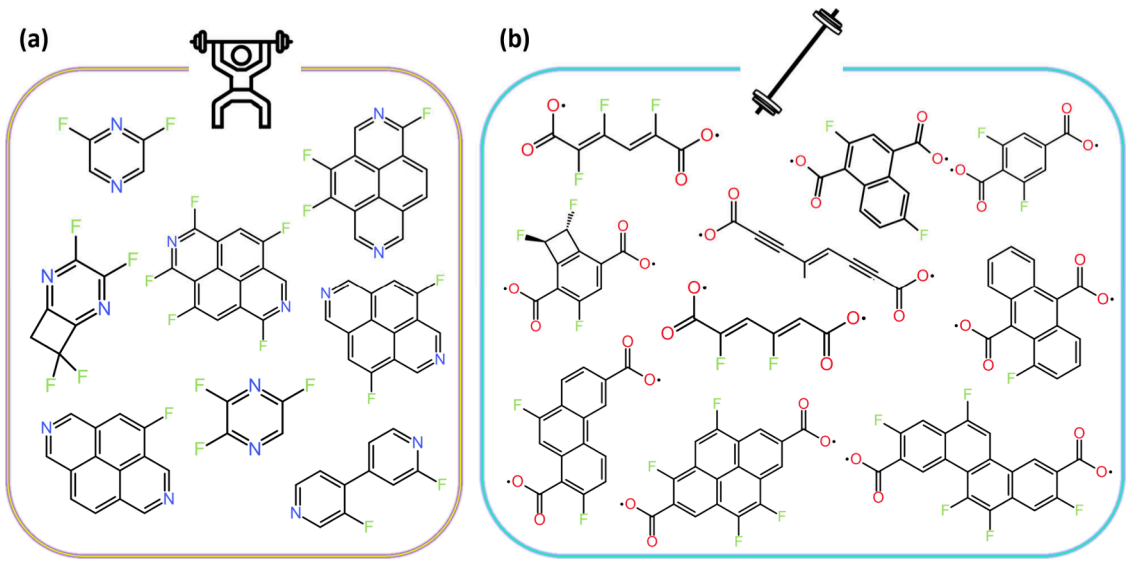

Figure 5. Typical (a) pillar groups and (b) organic linkers in the top 19 FMOFs.

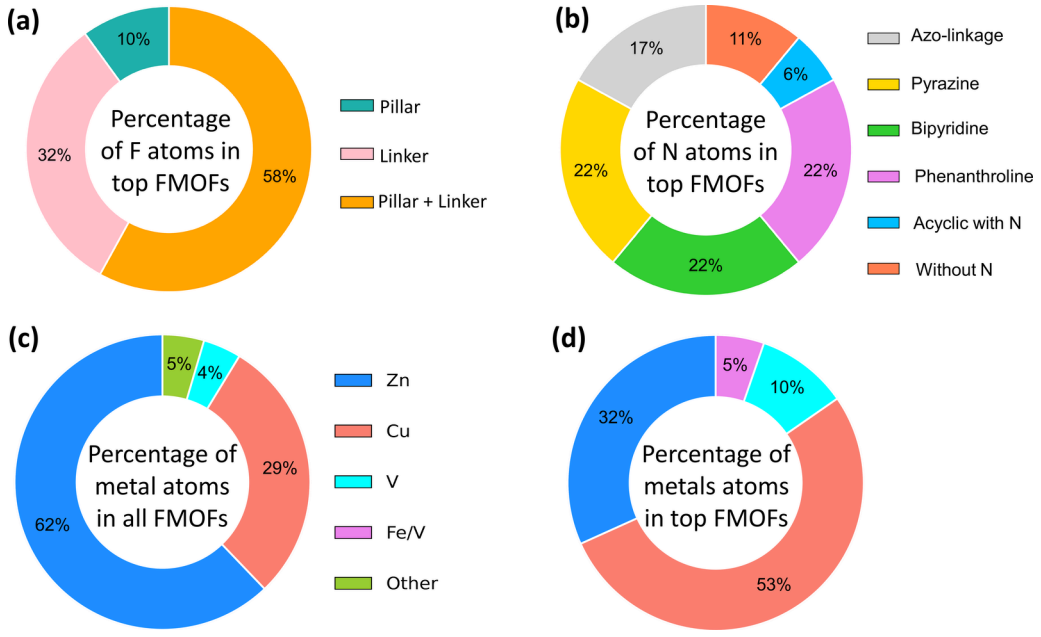

Figure 6. (a) Percentage of F atoms in the top 19 FMOFs. (b) Percentage of N atoms in the top 19 FMOFs. (c) Percentage of metal atoms in all 5061 FMOFs. (d) Percentage of metal atoms in the top 19 FMOFs.

appreciable amount of H_2O adsorption (0.14 and 1.84 mmol·g^{-1}). S_{CO_2/N_2} in the 19 FMOFs are all very high, ranging from 101 to 47 708. Particularly, hMOF-5033915 and hMOF-16702 exhibit the highest S_{CO_2/N_2} (47 708 and 18 244), but their N_{CO_2} values are not high (2.02 and 2.54 mmol·g^{-1}). Considering the effect of H_2O, hMOF-35835 has the highest H_2O adsorption N_{H_2O}(10.09 mmol·g^{-1}), the lowest S_{CO_2/N_2} (101.66), and the lowest S_{CO_2/H_2O} (0.05). Among the top 19 FMOFs, S_{CO_2/H_2O} in six FMOFs exceed 15 with the highest value of ∼100. In other FMOFs, however, S_{CO_2/H_2O} are not very high and even lower than 1; this reflects the challenge of CO_2 capture in the presence of H_2O.

As shown in Figure S2, $Q_{st(CO_2)}$ in most of the top 19 FMOFs are greater than $Q_{st(H_2O)}$, as also previously reported.[41,42] We should note that $Q_{st(CO_2)}$ and $Q_{st(H_2O)}$ in Figure S2 are based on the adsorption of the $CO_2/N_2/H_2O$ mixture (0.124/0.850/0.026) at 1 bar, not at infinite dilution as in Figure 3. Consequently, $Q_{st(H_2O)}$ in many FMOFs are >42 kJ/mol due to cooperative interactions, despite their $Q^{o}_{st(H_2O)} \leq$ 42 kJ/mol. In addition, GCMC simulations were also conducted to calculate the adsorption isotherms of pure CO_2 and N_2, CO_2/N_2 mixture (i.e., dry flue gas), and $CO_2/N_2/H_2O$ mixture (i.e., wet flue gas) up to 1 bar in the top 19 FMOFs. As illustrated in Figure S3, CO_2 exhibits type-I adsorption behavior in all 19 FMOFs, indicating favorable CO_2–framework interaction. N_2 adsorption is weak with a nearly linear relationship versus pressure (i.e., in Henry's region). By comparing the adsorption isotherms of dry and wet flue gas (Figures S4–S5), we find that CO_2 adsorption is affected

https://doi.org/10.1021/cbe.4c00111
Chem Bio Eng. 2024, 1, 970–978

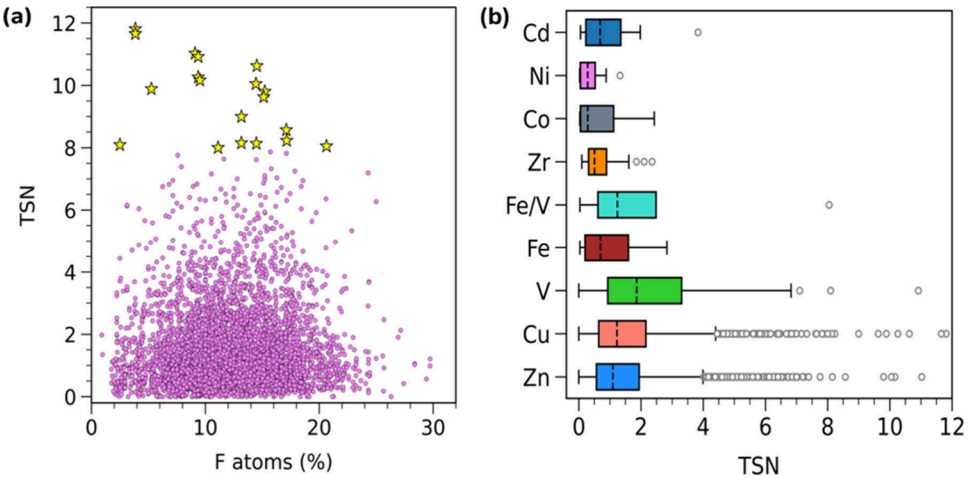

Figure 7. (a). TSN versus percentage of F atoms. The top 19 FMOFs are shown by stars. (b). TSN in 5061 FMOFs with different metal types. For boxplots, the box is drawn from the first quartile to the third quartile with a dashed line denoting the median.

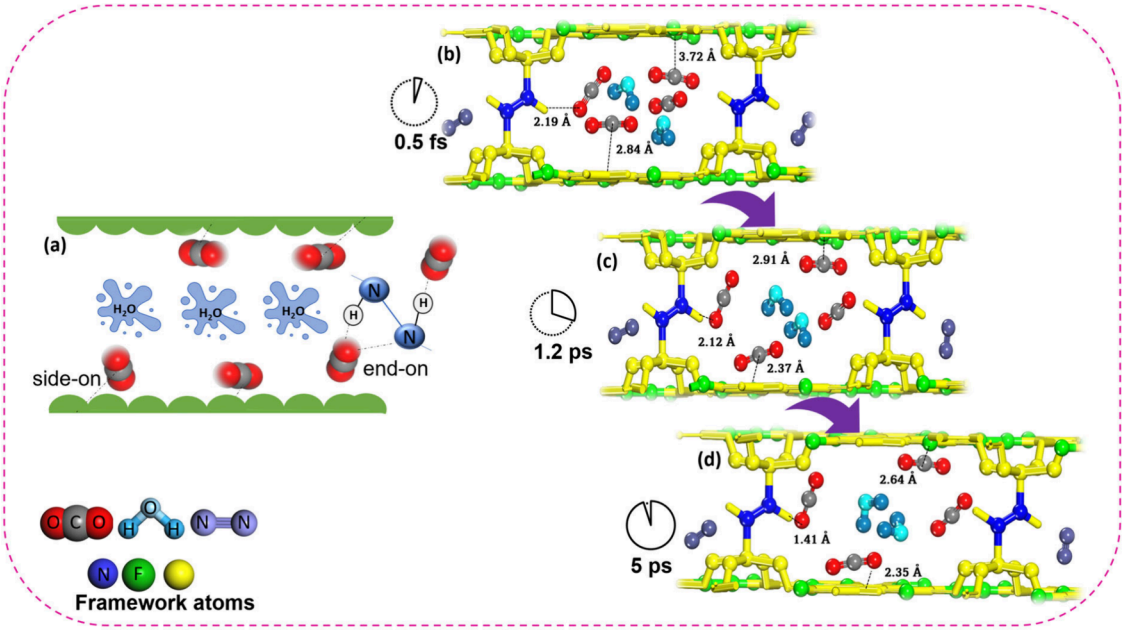

Figure 8. (a) Schematic illustration for CO_2 interaction with hydrazine in hMOF-35835. (b–d) FPMD simulation snapshots in hMOF-35835 at different times.

marginally by H_2O in many of the top FMOFs but significantly in hMOF-35835, hMOF-26522, hMOF-27207, hMOF-24459, and hMOF-34934. In these FMOFs, N_{CO_2} at 1 bar are reduced substantially under a wet condition (Figure S6).

3.3. Chemical Constituents in Top FMOFs. Figure 5 illustrates the typical pillar groups and organic linkers in the top FMOFs. All of the pillar groups comprise F and N atoms, while F atoms also exist in most of the organic linkers. It is thus instructive to quantitatively analyze the role of these constituent atoms in CO_2 capture. F atoms in FMOFs can be considered as three categories: (i) in the pillar group, (ii) in the organic linker, and (iii) in both the pillar group and organic linker. As shown in Figure 6a, among the top 19 FMOFs, 10%, 32%, and 58% FMOFs have F atoms in the three categories, respectively; with the highest percentage in category (iii). This reveals that F atoms of category (iii) present in both the pillar group and organic linker are more preferential for CO_2 capture. Therefore, the position of F atom in FMOFs affects CO_2 capture. This is further corroborated by the radial distribution functions between F atom and C_{CO2} in the top 19 FMOFs (Figure S7). Peaks are observed in some of the 19 FMOFs demonstrating strong F–CO_2 interaction but not in others, primarily depending on whether F atom is exposed to the pore center or not. Nevertheless, as presented in Figure 7a, the amount or percentage of F atoms is not distinctly associated with the capture performance (i.e., TSN).

Among the top 19 FMOFs, near 90% have N atoms in pillar groups rather than in organic linkers. The only exception is VOFFIVE_3_Fe with pyrazine as its linker. The pillar groups in FMOFs can be classified into cyclic (such as pyrazine, bipyridine, and phenanthroline), acyclic, azo-linkage, and finally the one without N. As shown in Figure 6b, an equal percentage is observed by different cyclic pillar groups including pyrazine (22%), bipyridine (22%), and phenanthroline (22%) in the top FMOFs, whereas azo-linkage has a smaller percentage (17%). This suggests that N atoms in cyclic

https://doi.org/10.1021/cbe.4c00111
Chem Bio Eng. 2024, 1, 970–978

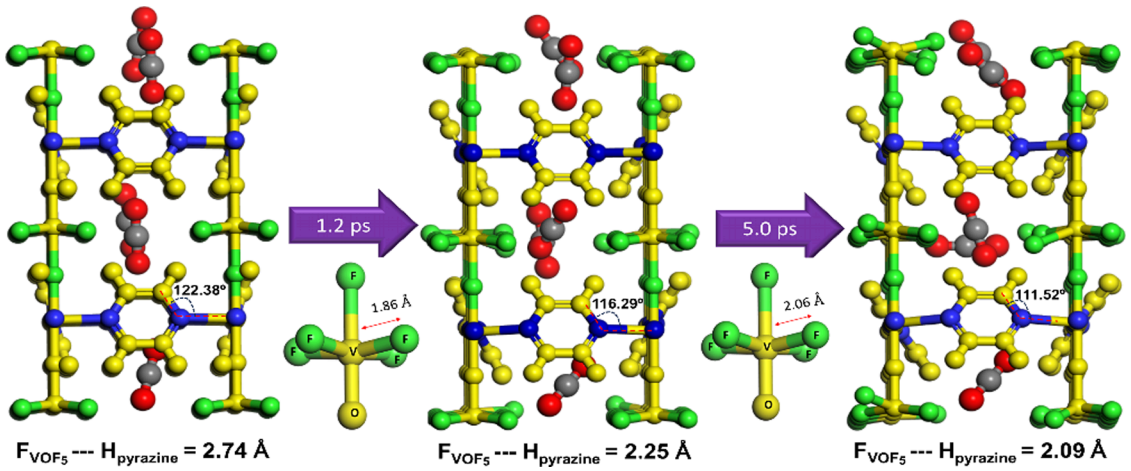

Figure 9. FPMD simulation snapshots for the rotation of pyrazine in VOFFIVE-3_Fe. F: green, N: blue, other framework atoms: yellow, gray, and red: C and O of CO_2.

groups are more favorable to CO_2 capture in the presence of humidity.

In addition to pillar groups and organic linkers, metal atoms in FMOFs also play an important role in CO_2 capture. Among 5061 FMOFs, Figure 6c shows that 3d transition metal Zn (62%) is the most popular, followed by Cu (29%), V (4%), and others (5%). In the top 19 FMOFs, as indicated by Figure 6d, Cu-based FMOFs count for the highest percentage (53%) compared to Zn (32%), V (10%), and Fe/V (5%). As shown in Figure 7b, V-based FMOFs exhibit notable overall performance, followed by Cu- and Zn-FMOFs.

3.4. Hydrostability and CO_2−Framework Interaction in Top FMOFs. Hydrostability and CO_2−framework interaction in top FMOFs are analyzed from FPMD simulation results. We first consider top FMOFs (hMOF-35835, hMOF-5063923, hMOF-5063926, and hMOF-28562) with N-containing pillar groups such as hydrazine and azo-linkage. As exemplified in hMOF-35835, the terminal hydrogen atoms of hydrazine are exposed to the pore center. During FPMD simulation, the protruded hydrogen atoms involve end-on interaction with CO_2, as schematically illustrated in Figure 8a. From the simulation snapshots in Figure 8b−8d, we observe that the distance between the O atom of CO_2 and the H atom of hydrazine is reduced from initial 2.19 to 1.41 Å after 5 ps. A similar trend is also seen in the distance between the C atom of CO_2 and the F atom of the framework, which is reduced from 3.72 to 2.64 Å. With the presence of hydrazine groups and F atoms, CO_2 molecules are closely attracted to the pore wall, while H_2O molecules are located in the pore center. The F-decorated framework provides a hydrophobic environment and maintains hydrostability in the presence of H_2O.

A few top FMOFs like hMOF-5063923, hMOF-5063926, and hMOF-28562 are connected via azo-linkage. The simulation snapshots in Figures S8−S10 reveal that these FMOFs are hydrostable after 5 ps simulation and guest molecules (CO_2, N_2, and H_2O) reside in the pore center of each FMOF. The locations of CO_2 and H_2O molecules are slightly perturbed during FPMD simulation. In hMOF-5063923, a weak interaction exists between CO_2 and F atom at the initial stage. After 5 ps, the distance between the C atom of CO_2 and the F atom is reduced from 3.83 to 3.69 Å (Figure S8), and CO_2 molecules tend to align in a straight line and interact strongly with the F-decorated pore wall. A similar trend occurs in its configurational isomer hMOF-5063926, in which the CO_2−F distance is reduced marginally from 3.98 to 3.94 Å (Figure S9). In hMOF-28562, a substantial reduction is observed in CO_2−F distance, from initial 4.15 to 2.82 Å (Figure S10). Due to the existence of multiple favorable adsorption sites, hMOF-28562 interacts with CO_2 more strongly compared to hMOF-5063923 and hMOF-5063923; thus, CO_2 is comparatively closer to F atom with a distance of 2.82 Å.

It is also interesting to investigate the hydrostability and CO_2 interaction in top FMOFs such as hMOF-34259, hMOF-24459, hMOF-27207, VOFFIVE-3_Fe, hMOF-1002619, hMOF-28016, and hMOF-36835, where the percentage of F atom gradually decreases. Figures S11−S13 show the initial and final simulation snapshots in hMOF-34259, hMOF-24459, and hMOF-27207. These FMOFs possess exceptional structural stability during CO_2 adsorption in the presence of H_2O. As shown in Figure S11, F-rich hMOF-34259 exerts a high affinity for CO_2 molecules with a short CO_2−F distance of 2.39 Å after 5 ps. The favorable side-on interaction between CO_2 and F atom results in a straight alignment of CO_2 molecules in the pore center. A similar pattern is noticed in hMOF-24459 and hMOF-27207, where the adsorption site near F atom enhances CO_2 adsorption; nevertheless, CO_2−F distance is longer, 3.10 Å in hMOF-24459 (Figure S12) and 2.89 Å in hMOF-27207 (Figure S13).

As another top FMOF with a high percentage of F atoms, VOFFIVE-3_Fe displays a slight configurational change during FPMD simulation. The square-pillared VOFFIVE-3_Fe consists of N-containing pyrazine coordinated with a VOF_5 pillar group to form a 3D network. It is evident from Figure 9 that the pyrazine in VOFFIVE-3_Fe is rotated by 11° toward the pore center after 5 ps FPMD simulation, thus achieving an energetically favorable position. F atoms in the equatorial VOF_5 pillar group become closer to the H atoms of pyrazine after the rotation. Specifically, the distance of F_{VOF5}−$H_{pyrazine}$ is reduced from initial 2.74 Å to a final 2.09 Å. Consequently, the pore size is adjusted to accommodate CO_2 rather than H_2O and maintains the adsorption sites in the pore. A similar trend was previously observed in KAUST-7 (NbOFFIVE-1-Ni) with reducing pore size and selective sieving of guest molecules.[22]

In the top FMOFs (hMOF-1002619, hMOF-28016, and hMOF-36835) with a low percentage of F atoms, Figures

https://doi.org/10.1021/cbe.4c00111
Chem Bio Eng. 2024, 1, 970−978

S14–S16 generally indicate weak interaction between CO_2 and the framework. However, hMOF-1002619 exhibits relatively stronger interaction with CO_2–F distance reduced from 4.94 to 2.36 Å during FPMD simulation. In hMOF-34934, CO_2 becomes closer to F atom with a distance of ∼2.00 Å during FPMD simulation (Figure S17). In other top FMOFs including hMOF-16702, hMOF-1002454, hMOF-26522, hMOF-5033915, hMOF-31797, hMOF-5033608, and hMOF-36776, no explicit structural change is observed (Figures S18–S24) throughout the entire FPMD simulation, thus implying their hydrostability in the presence of coadsorbed CO_2 and H_2O. Additionally, the PLDs of the top 19 MOFs during FPMD simulations are shown in Figure S25. In most of the FMOFs, the PLDs are slightly reduced within 5 ps due to the interactions between framework and guest molecules (CO_2, N_2, and H_2O), suggesting that the frameworks largely maintain structural integrity.

4. CONCLUSIONS

We conducted multiscale computational screening to identify hydrostable FMOFs capable of CO_2 capture from a wet flue gas. Among 5061 FMOFs, 19 are shortlisted as top candidates. These top FMOFs possess PLD ranging from 2.75 to 4.25 Å, porosity ϕ from 0.2 to 0.3, CO_2 capacity N_{CO_2} from 2.02 and 4.14 mmol·g^{-1}, S_{CO_2/N_2} from 101 to 47 708, and S_{CO_2/H_2O} ranging between 0.05 and 100. All the pillar groups in the top FMOFs contain F and N atoms, while F atoms also exist in many of the organic linkers. It is unravelled that the position of F atom, rather than the amount, influences CO_2 adsorption; and N-containing pillar groups facilitate CO_2 capture in the presence of humidity. Among the top 19 FMOFs, Cu-based FMOFs have the highest percentage compared to Zn-, V-, and Fe-counterparts. From FPMD simulations, the top FMOFs are hydrostable in the presence of coadsorbed CO_2 and H_2O. Therefore, fluorination provides a hydrophobic environment and maintains hydrostability. Two unique behaviors are observed during FPMD simulations for structural integrity and CO_2 interaction-framework in the top FMOFs. First, strong interaction exists between CO_2 and F atom; thus, CO_2 is effectively trapped in the framework, which is particularly pronounced in FMOFs with N-containing pillar groups. Second, as observed in VOFFIVE-3_Fe with pyrazine, the pore size is adjusted via the rotation of pyrazine to accommodate CO_2 instead of H_2O. These findings suggest the potential directions toward future development of hydrostable MOFs for CO_2 capture in a realistic condition. Finally, it is worthwhile to note that in this study, only material properties (adsorption capacity and selectivity) are used to assess their performance for CO_2 capture; nevertheless, a more sophisticated approach including process and system-level optimization should be integrated for holistic assessment.[43]

ASSOCIATED CONTENT

Supporting Information

The Supporting Information is available free of charge at https://pubs.acs.org/doi/10.1021/cbe.4c00111.

Adsorption performance of FMOFs in different databases, $Q_{st(CO_2)}$ and $Q_{st(H_2O)}$ in top 19 FMOFs, crystal structures of top 19 FMOFs, pure CO_2 and N_2 adsorption isotherms, binary CO_2/N_2 adsorption isotherms, ternary $CO_2/N_2/H_2O$ adsorption isotherms, CO_2 adsorption capacities in top 19 FMOFs under dry and wet conditions, radial distribution functions of F–C_{CO_2} in top 19 FMOFs, FPMD simulation snapshots, and PLDs of top 19 FMOFs during FPMD simulations (PDF)

AUTHOR INFORMATION

Corresponding Author

Jianwen Jiang − *Department of Chemical and Bimolecular Engineering, National University of Singapore, 117576, Singapore;* orcid.org/0000-0003-1310-9024; Email: chejj@nus.edu.sg

Authors

Athulya S. Palakkal − *Department of Chemical and Bimolecular Engineering, National University of Singapore, 117576, Singapore;* orcid.org/0000-0001-9812-9088

Saad Aldin Mohamed − *Department of Chemical and Bimolecular Engineering, National University of Singapore, 117576, Singapore;* orcid.org/0000-0002-7420-4490

Complete contact information is available at: https://pubs.acs.org/10.1021/cbe.4c00111

Notes

The authors declare no competing financial interest.

ACKNOWLEDGMENTS

We gratefully acknowledge the A*STAR LCER-FI projects (LCERFI01-0015 U2102d2004 and LCERFI01-0033 U2102d2006) and the National Research Foundation Singapore (NRF-CRP26-2021RS-0002) for financial support and the National University of Singapore and the National Supercomputing Centre (NSCC) Singapore for computational resources.

REFERENCES

(1) Monastersky, R. Global Carbon Dioxide Levels Near Worrisome Milestone. *Nature.* **2013**, *497*, 13–14.

(2) Weaver, A. J. Toward the Second Commitment Period of the Kyoto Protocol. *Science.* **2011**, *332*, 795–796.

(3) Figueroa, J. D.; Fout, T.; Plasynski, S.; McIlvried, H.; Srivastava, R. D. Advances in CO_2 Capture Technology-The U.S. Department of Energy's Carbon Sequestration Program. *Int. J. Greenh. Gas Control.* **2008**, *2*, 9–20.

(4) Yang, H.; Xu, Z.; Fan, M.; Gupta, R.; Slimane, R. B.; Bland, A. E.; Wright, I. Progress in Carbon Dioxide Separation and Capture: A Review. *J. Environ. Sci.* **2008**, *20*, 14–27.

(5) Kitagawa, S. Porous Materials and the Age of Gas. *Angew. Chem., Int. Ed.* **2015**, *127*, 10834–10835.

(6) Sumida, K.; Rogow, D. L.; Mason, J. A.; McDonald, T. M.; Bloch, E. D.; Herm, Z. R.; Bae, T. H.; Long, J. R. Carbon Dioxide Capture in Metal-Organic Frameworks. *Chem. Rev.* **2012**, *112*, 724–781.

(7) Liu, J.; Thallapally, P. K.; Mc Grail, B. P.; Brown, D. R.; Liu, J. Progress in Adsorption-Based CO_2 Capture by Metal-Organic Frameworks. *Chem. Soc. Rev.* **2012**, *41*, 2308–2322.

(8) Yu, J.; Xie, L. H.; Li, J. R.; Ma, Y.; Seminario, J. M.; Balbuena, P. B. CO_2 Capture and Separations Using MOFs: Computational and Experimental Studies. *Chem. Rev.* **2017**, *117*, 9674–9754.

(9) Mangano, E.; Kahr, J.; Wright, P. A.; Brandani, S. Accelerated Degradation of MOFs under Flue Gas Conditions. *Faraday Discuss.* **2016**, *192*, 181–195.

(10) Liu, J.; Benin, A. I.; Furtado, A. M. B.; Jakubczak, P.; Willis, R. R.; Levan, M. D. Stability Effects on CO_2 Adsorption for the DOBDC

Series of Metal-Organic Frameworks. *Langmuir.* **2011**, *27*, 11451−11456.
(11) Chung, Y. G.; Camp, J.; Haranczyk, M.; Sikora, B. J.; Bury, W.; Krungleviciute, V.; Yildirim, T.; Farha, O. K.; Sholl, D. S.; Snurr, R. Q. Computation-Ready, Experimental Metal-Organic Frameworks: A Tool to Enable High-Throughput Screening of Nanoporous Crystals. *Chem. Mater.* **2014**, *26*, 6185−6192.
(12) Wilmer, C. E.; Leaf, M.; Lee, C. Y.; Farha, O. K.; Hauser, B. G.; Hupp, J. T.; Snurr, R. Q. Large-Scale Screening of Hypothetical Metal-Organic Frameworks. *Nat. Chem.* **2012**, *4*, 83−89.
(13) Wilmer, C. E.; Farha, O. K.; Bae, Y. S.; Hupp, J. T.; Snurr, R. Q. Structure-Property Relationships of Porous Materials for Carbon Dioxide Separation and Capture. *Energy Environ. Sci.* **2012**, *5*, 9849−9856.
(14) Qiao, Z.; Peng, C.; Zhou, J.; Jiang, J. High-Throughput Computational Screening of 137953 Metal-Organic Frameworks for Membrane Separation of a $CO_2/N_2/CH_4$ Mixture. *J. Mater. Chem. A* **2016**, *4*, 15904−15912.
(15) Qiao, Z.; Xu, Q.; Jiang, J. Computational Screening of Hydrophobic Metal-Organic Frameworks for the Separation of H_2S and CO_2 from Natural Gas. *J. Mater. Chem. A* **2018**, *6*, 18898−18905.
(16) Avci, G.; Erucar, I.; Keskin, S. Do New MOFs Perform Better for CO_2 Capture and H_2 Purification? Computational Screening of the Updated MOF Database. *ACS Appl. Mater. Interfaces.* **2020**, *12*, 41567−41579.
(17) Majumdar, S.; Moosavi, S. M.; Jablonka, K. M.; Ongari, D.; Smit, B. Diversifying Databases of Metal-Organic Frameworks for High-Throughput Computational Screening. *ACS Appl. Mater. Interfaces.* **2021**, *13*, 61004−61014.
(18) Boyd, P. G.; Chidambaram, A.; García-Díez, E. P. I. C.; Daff, T. D.; Bounds, R.; Gladysiak, A.; Schouwink, P.; Moosavi, S. M.; Maroto-Valer, M. M.; Reimer, J. A.; Navarro, J. A. R.; Woo, T. K.; Garcia, S.; Stylianou, K. C.; Smit, B.; Ireland, C. P. Data-Driven Design of Metal-Organic Frameworks for Wet Flue Gas CO_2 Capture. *Nature.* **2019**, *576*, 253−256.
(19) Yang, C.; Wang, X.; Omary, M. A. Fluorous Metal-Organic Frameworks for High-Density Gas Adsorption. *J. Am. Chem. Soc.* **2007**, *129*, 15454−15455.
(20) Pachfule, P.; Banerjee, R. Metal−Organic Frameworks: Fluorinated Frameworks. *Encyclopedia of Inorganic and Bioinorganic Chemistry*; Scott, R. A., Ed.; John Wiley & Sons, Ltd.: New York, 2014; pp 1−14.
(21) Bhatt, P. M.; Belmabkhout, Y.; Cadiau, A.; Adil, K.; Shekhah, O.; Shkurenko, A.; Barbour, L. J.; Eddaoudi, M. A Fine-Tuned Fluorinated MOF Addresses the Needs for Trace CO_2 Removal and Air Capture Using Physisorption. *J. Am. Chem. Soc.* **2016**, *138*, 9301−9307.
(22) Cadiau, A.; Adil, K.; Bhatt, P. M.; Belmabkhout, Y.; Eddaoudi, M. A Metal-Organic Framework-Based Splitter for Separating Propylene from Propane. *Science.* **2016**, *353*, 137−140.
(23) Cadiau, A.; Belmabkhout, Y.; Adil, K.; Bhatt, P. M.; Pillai, R. S.; Shkurenko, A.; Martineau-Corcos, C.; Maurin, G.; Eddaoudi, M. Hydrolytically Stable Fluorinated Metal-Organic Frameworks for Energy-Efficient Dehydration. *Science.* **2017**, *356*, 731−735.
(24) Deria, P.; Mondloch, J. E.; Tylianakis, E.; Ghosh, P.; Bury, W.; Snurr, R. Q.; Hupp, J. T.; Farha, O. K. Perfluoroalkane Functionalization of NU-1000 via Solvent-Assisted Ligand Incorporation: Synthesis and CO_2 Adsorption Studies. *J. Am. Chem. Soc.* **2013**, *135*, 16801−16804.
(25) Moghadam, P. Z.; Ivy, J. F.; Arvapally, R. K.; Dos Santos, A. M.; Pearson, J. C.; Zhang, L.; Tylianakis, E.; Ghosh, P.; Oswald, I. W.; Kaipa, U.; et al. Adsorption and Molecular Siting of CO_2, Water and Other Gases in the Superhydrophobic, Flexible Pores of FMOF-1 from Experiment and Simulation. *Chem. Sci.* **2017**, *8*, 3989−4000.
(26) Di, T.; Yoshida, Y.; Otake, K.; Kitagawa, S.; Kitagawa, H. Increased CO_2/N_2 Selectivity by Stepwise Fluorination in Isoreticular Ultramicroporous Metal-Organic Frameworks. *Chem. Sci.* **2024**, *15*, 9641−9648.
(27) Gu, C.; Yu, Z.; Liu, J.; Sholl, D. S. Construction of an Anion-Pillared MOF Database and the Screening of MOFs Suitable for Xe/Kr Separation. *ACS Appl. Mater. Interfaces.* **2021**, *13*, 11039−11049.
(28) Chung, Y. G.; Haldoupis, E.; Bucior, B. J.; Haranczyk, M.; Lee, S.; Zhang, H.; Vogiatzis, K. D.; Milisavljevic, M.; Ling, S.; Camp, J. S.; Slater, B.; Siepmann, J. I.; Sholl, D. S.; Snurr, R. Q. Advances, Updates, and Analytics for the Computation-Ready, Experimental Metal- Organic Framework Database: CoRE MOF 2019. *J. Chem. Eng. Data* **2019**, *64*, 5985−5998.
(29) Willems, T. F.; Rycroft, C. H.; Kazi, M.; Meza, J. C.; Haranczyk, M. Algorithms and Tools for High-Throughput Geometry-Based Analysis of Crystalline Porous materials. *Microporous Mesoporous Mater.* **2012**, *149*, 134−141.
(30) Rappé, A. K.; Casewit, C. J.; Colwell, K. S.; Goddard, W. A.; Skiff, W. M. UFF, A Full Periodic Table Force Field for Molecular Mechanics and Molecular Dynamics Simulations. *J. Am. Chem. Soc.* **1992**, *114*, 10024−10035.
(31) Mayo, S. L.; Olafson, B. D.; Goddard, W. A. DREIDING: A Generic Force Field for Molecular Simulations. *J. Phys. Chem. A* **1990**, *94*, 8897−8909.
(32) Kancharlapalli, S.; Gopalan, A.; Haranczyk, M.; Snurr, R. Q. Fast and Accurate Machine Learning Strategy for Calculating Partial Atomic Charges in Metal-Organic Frameworks. *J. Chem. Theory. Comput.* **2021**, *17*, 3052−3064.
(33) Potoff, J. J.; Siepmann, J. I. Vapor-Liquid Equilibria of Mixtures Containing Alkanes, Carbon Dioxide, and Nitrogen. *AIChE J.* **2001**, *47*, 1676−1682.
(34) Jorgensen, W. L.; Chandrasekhar, J.; Madura, J. D.; Impey, R. W.; Klein, M. L. Comparison of simple potential functions for simulating liquid water. *J. Chem. Phys.* **1983**, *79*, 926−935.
(35) Datar, A.; Witman, M.; Lin, L.-C. Monte Carlo Simulations for Water Adsorption in Porous Materials: Best Practices and New Insights. *AIChE J.* **2021**, *67*, No. e17447.
(36) Dubbeldam, D.; Calero, S.; Ellis, D. E.; Snurr, R. Q. RASPA: Molecular Simulation Software for Adsorption and Diffusion in Flexible Nanoporous Materials. *Mol. Simul.* **2016**, *42*, 81−101.
(37) Kühne, T. D.; Iannuzzi, M.; Del Ben, M.; Rybkin, V. V.; Seewald, P.; Stein, F.; Laino, T.; Khaliullin, R. Z.; Schütt, O.; Schiffmann, F.; Golze, D.; Wilhelm, J.; Chulkov, S.; Bani-Hashemian, M. H.; Weber, V.; Borštnik, U.; Taillefumier, M.; Jakobovits, A. S.; Lazzaro, A.; Pabst, H.; Müller, T.; Schade, R.; Guidon, M.; Andermatt, S.; Holmberg, N.; Schenter, G. K.; Hehn, A.; Bussy, A.; Belleflamme, F.; Tabacchi, G.; Glöß, A.; Lass, M.; Bethune, I.; Mundy, C. J.; Plessl, C.; Watkins, M.; VandeVondele, J.; Krack, M.; Hutter, J. CP2K: An Electronic Structure and Molecular Dynamics Software Package Quickstep: Efficient and Accurate Electronic Structure Calculations. *J. Chem. Phys.* **2020**, *152*, 194103.
(38) Perdew, J. P. DFT Approximations for the Correlation Energy of the Inhomogeneous Electron Gas. *Phys. Rev. B* **1986**, *33*, 8822−8824.
(39) Perdew, J. P.; Burke, K.; Ernzerhof, M. Generalized Gradient Approximation Made Simple. *Phys. Rev. Lett.* **1996**, *77*, 3865−3868.
(40) Grimme, S.; Antony, J.; Ehrlich, S.; Krieg, H. A Consistent and Accurate Ab Initio Parametrization of Density Functional Dispersion Correction (DFT-D) for the 94 Elements H-Pu. *J. Chem. Phys.* **2010**, *132*, 154104.
(41) Li, S.; Chung, Y. G.; Snurr, R. Q. High-Throughput Screening of Metal-Organic Frameworks for CO_2 Capture in the Presence of Water. *Langmuir* **2016**, *32*, 10368−10376.
(42) Kancharlapalli, S.; Snurr, R. Q. High-Throughput Screening of the CoRE-MOF-2019 Database for CO_2 Capture from Wet Flue Gas: A Multi-Scale Modeling Strategy. *ACS Appl. Mater. Interfaces.* **2023**, *15*, 28084−28092.
(43) Farmahini, A. H.; Krishnamurthy, S.; Friedrich, D.; Brandani, S.; Sarkisov, L. Performance-Based Screening of Porous Materials for Carbon Capture. *Chem. Rev.* **2021**, *121*, 10666−10741.

https://doi.org/10.1021/cbe.4c00111
Chem Bio Eng. 2024, 1, 970−978